Molybdenum thin films fabricated by rf and dc sputtering for Cu(In,Ga)Se_2 solar cell applications

Beibei Guo (郭贝贝)[1], Yaoming Wang (王耀明)[2], Xiaolong Zhu (朱小龙)[2], Mingsheng Qin (秦明升)[2], Dongyun Wan (万冬云)[1,*], and Fuqiang Huang (黄富强)[2]

[1]*School of Materials Science and Engineering, Shanghai University, Shanghai 200444, China*

[2]*CAS Key Laboratory of Materials for Energy Conversion, Shanghai Institute of Ceramics, Chinese Academy of Sciences, Shanghai 200050, China*

**Corresponding author: echowandy@shu.edu.cn*

Received October 31, 2015; accepted February 4, 2016; posted online March 21, 2016

Molybdenum (Mo) thin films, most commonly used as electrical back contacts in Cu(In, Ga)Se_2 (CIGS) solar cells, are deposited by rf and dc magnetron sputtering in identical systems to study the discrepancy and growth mechanisms of the two sputtering techniques. The results reveal that though different techniques generally deposit films with different characteristic properties, Mo films with similar structural and physical properties can be obtained at respective suitable deposition conditions. Highly adhesive and conductive Mo films on soda lime glass are further optimized, and the as-fabricated solar cells reach efficiencies as high as 9.4% and 9.1% without an antireflective layer.

OCIS codes: 310.1860, 040.5350, 350.6050.
doi: 10.3788/COL201614.043101.

The Cu(In, Ga)Se_2 (CIGS)-based chalcopyrite material is one of the most promising absorber material because the CIGS solar cell maintains the highest photovoltaic efficiency of 21.7% among thin film solar cells[1]. In the common configuration of CIGS thin film solar cells, molybdenum (Mo) films have been selected as the best back ohmic contact. The reasons are that not only is itchemically stable for the critical Cu-In-Ga alloy and the precursor gas of H_2Se or Se, but its work function matches the absorber CIGS[2,3] well. Extensive research has been carried out on the deposition of Mo thin films by the magnetron sputtering technique. Currently, there have been two magnetron sputtering techniques generally used, either dc-based[4–11] or rf-based[12–18]. But so far few comparative and systematic investigations have been reported.

Although the dc and rf techniques are different, the energetic and kinetics of the film growth are essentially similar. They are closely related with the following common adjusting parameters. Namely, power, atmosphere, pressure, target-hold distance, substrate temperature, deposition duration, etc. These parameters play a critical role in the nucleation and growth process, and thus the microstructure and physical properties of the Mo films. From this viewpoint, the dc and rf techniques can both grow Mo films with a similar morphology and electrical conductivity as long as it is at their respective suitable deposition conditions. At the same time, another important factor to affect the structure and properties of Mo films is the deposition procedure. Our recent study[19] and related allied investigations have shown that the two-step deposition process will greatly favor the formation of the expected Mo films. In the two-step process, first the high-pressure deposition will enhance the adhesion between the substrate and the films while the second step, low-pressure deposition, has a rather fast film growth rate and tends to form the textured surfaces. In this study, a two-step deposition has been purposely adopted to form the Mo films in order to validate our conclusions in a more meaningful but uncertain process.

In order to conduct the comparative study, rf and dc magnetron sputtering techniques have been applied in the same system with the two-step process as a function of different sputtering powers, which are found to be the most critical variable. The structural, morphological, and physical properties of the rf- and dc-sputtered Mo films have been, respectively, studied and compared. The results indicate that though a different process grows its characteristic Mo films, the films with quite a similar structural and physical properties could be obtained by different dc and rf techniques at respectively suitable deposition conditions. The Mo films at the optimal conditions have been further assembled into CIGS solar cells as back contacts, and an efficiency as high as 9.4% is obtained. The value confirms that the as-prepared Mo films are good adhesives and highly conductive, and suitable to be used in CIGS solar cells.

The whole experimental process was carried out in a JGP450 magnetron sputtering system. An unthrottled base pressure of 2.0×10^{-4} Pa was used and achieved by a combined vacuum system of a mechanical pump and a turbomolecular pump. The ϕ 50.8 mm Mo target has a purity of 99.9 wt% and soda-lime glass is used as the substrates. The deposition of the Mo thin films was done at room temperature by a two-step magnetron sputtering process. The first sputtering step was for 15 min at a working pressure of 2.4 Pa, and the second step was for

 © 2016 Chinese Optics Letters

25 min at 0.6 Pa. An argon flow rate of 15 sccm was maintained during the deposition process. For investigating the growth mechanism and discrepancy of dc and rf techniques, two sets of experiments corresponding to the two-step sputtering above were conducted with a supplied power of 80, 100, and 120 W, respectively. Here no substrate bias was applied, and the related plasma potentials for dc sputtering were 115, 285, and 171 V, respectively, while 54, 62, and 71 V were used for rf sputtering. Solar cells with glass/Mo/CIGS/CdS/i-ZnO/ZnO:Al/Al grids structures were fabricated. The CdS buffer layers, with a nominal thickness of 50 nm, were deposited by chemical bath deposition (CBD). The window layers consisted of the i-ZnO with a thickness of 70 nm and a ZnO:Al layer with a thickness of 800 nm, and both layers were deposited by rf magnetron sputtering. The active sizes of the cells were 0.5 cm^2.

The x-ray diffraction (XRD) patterns of the Mo films were acquired on a Siemens D/MAX-2400 automated x-ray diffractometer with CuKα radiation. The surface and cross-section morphologies were observed on a field emission scanning electron microscope (FE-SEM, LEO-1530VP), and the surface roughness values were measured on an atomic force microscope (AFM, Seiko II SPI3800 V & spa300HV). A Dektak 150 surface profile system was used to measure the thickness of the Mo films. The electrical measurement was obtained at ambient temperature by the Van der Pauw method (Accent HL5500). The performance of the solar cells was evaluated under standard AM 1.5 illumination.

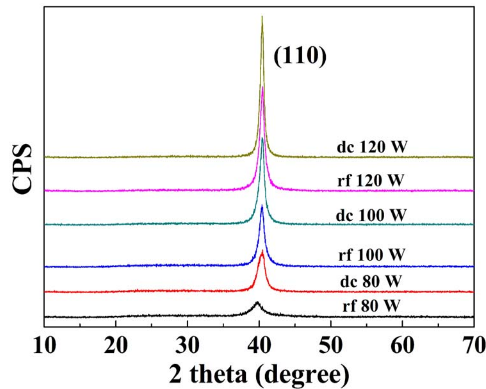

Fig. 1. XRD patterns of as-deposited Mo films prepared by dc and rf magnetron sputtering, respectively, as a function of the supplied power.

The XRD spectra of the as-deposited Mo thin films are shown in Fig. 1. Apparently, these films are all oriented along the (110) direction, which is consistent with the characteristic of the previously reported Mo films[6]. At 80 W supplied power, both dc- and rf-sputtered films are weak and broad, implying the low crystallization of the Mo films at both cases. As the supplied power increases, the full width at half-maximum (FWHM) of (110) in the respective Mo thin film decreases and the peak intensity (CPS) increases (see Table 1) in both cases. With 120 W of power supplied, the CPS significantly increases with a concomitant peak narrowing. This means that the crystallization of Mo films increases with increased sputtering power. This conclusion is expected considering that higher power generally favors the migration of Mo atoms and crystal growth. At the same time, the CPSs of the dc sputtering show systematically stronger than those of the rf sputtering, and the peak broadenings are narrower. For example, the CPS of the dc-100 W (1041.2) is higher than rf-100 W (688.9). Correspondingly, the deposition rate of the dc sputtering should be higher than the counterpart rf sputtering. This conclusion is verified by the film thickness measured by the Dektak 150 surface profile. dc-80 W induces a film thickness of 0.92 μm for total 40 mins' deposition, in contrast to 0.78 μm of the rf-80 W. The calculated deposition rate for dc-80 W is 23 nm/min, which is much higher than 19.5 nm/min of the rf-80 W. The intensity of the XRD diffraction peaks are found to be strongly affected by the film thickness. Table 1 summarizes the results of the two kinds of films with almost the same thickness (dc-100 W film of 1.38 μm and rf-120 W film of 1.42 μm), and their XRD results of the CPS and the peak broadening are also closer to each other and follow suit. That is to say, the XRD results exhibit the same trend for the two films with the same thickness. In other words, further power enhancement to a certain level in the rf case can compensate the above disparity and get a similar Mo crystallization. All the results above indicate that, through tuning the supplied power, the rf-sputtered films

Table 1. Structural and Electrical Properties of the As-Deposited Mo Films

Sample	CPS	FWHM (2θ)	Grain Size from AFM (nm)	Thickness (μm)	Roughness (Å)	$R(\Omega/\text{sq})$	ρ ($\mu\Omega \cdot \text{cm}$)
dc-80 W	471.6	0.559	37.5	0.92	22.3	0.31	63.7
dc-100 W	1041.2	0.409	68.7	1.38	49.6	0.23	28.1
dc-120 W	1620.6	0.280	158.3	1.85	162	0.14	10.2
rf-80 W	150.8	1.013	22.7	0.78	20.8	0.47	102.9
rf-100 W	688.9	0.442	42.1	1.13	26.6	0.38	56.6
rf-120 W	1059.4	0.401	70.6	1.42	50.3	0.24	27.8

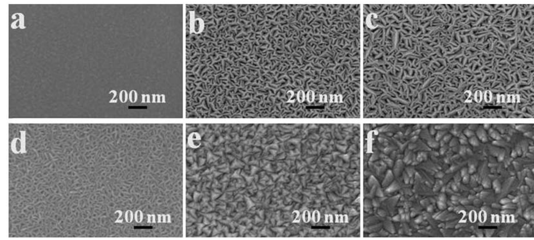

Fig. 2. SEM images of the Mo films prepared by dc and rf magnetron sputtering, respectively, with different supplied powers: (a) rf 80 W, (b) rf 100 W, (c) rf 120 W, (d) dc 80 W, (e) dc 100 W, and (f) dc 120 W.

can meet the structural properties of the dc-sputtered ones.

According to the XRD results, the sputtering method and the supplied power are expected to have a strong effect on the morphology of the films. The FE-SEM images of the as-deposited Mo film surface are shown in Fig. 2. It is clear that the surface roughness of the Mo film increases with the increase of the supply power. Simultaneously, the dc-sputtered films have a much more textured surface than the rf films at the same power value. The surface of the rf-80 W film is rather flat [Fig. 2(a)], but the fish-like texture can be observed for the dc-80 W film [Fig. 2(d)]. The surface textures in the dc-100 W [Fig. 2(e)] and dc-120 W [Fig. 2(f)] films are quite intense, much more than those of the corresponding rf-100 W [Fig. 2(b)] and rf-120 W films [Fig. 2(c)]. The surface textures reflect the grain growth of these Mo films. The dc-100 W and rf-120 W films consist of similarly large fish-like particles (70.6 nm in rf-120 W versus 68.7 nm in rf-100 W, as depicted in Table 1), but the surface morphologies are something different.

The surface textures can be further evaluated from the roughness of the Mo films, as shown in the AFM topographies (Fig. 3). The corresponding root mean square (RMS) roughness values are listed in Table 1. It can be

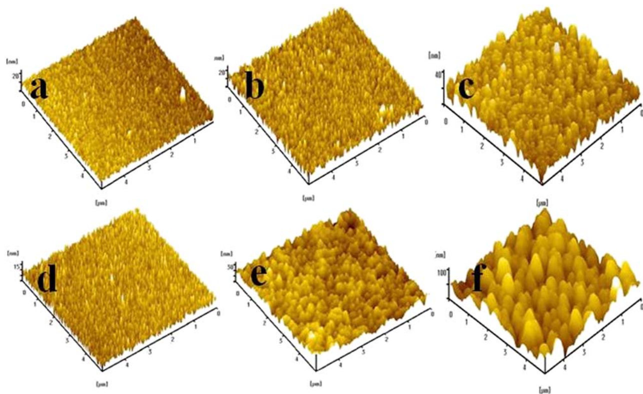

Fig. 3. AFM images of the Mo films prepared by dc and rf magnetron sputtering, respectively, with different supplied powers, revealing the differences in grain size and morphology: (a) rf 80 W, (b) rf 100 W, (c) rf 120 W, (d) dc 80 W, (e) dc 100 W, and (f) dc 120 W.

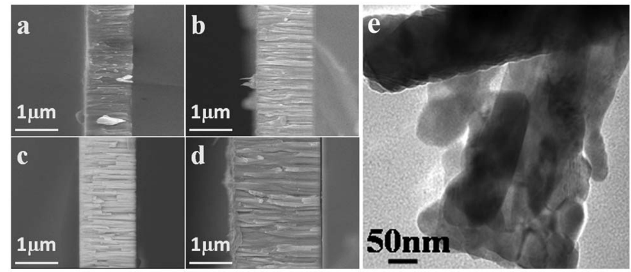

Fig. 4. Cross-sectional SEM images of the Mo films deposited at 100 and 120 W by rf and dc sputtering, respectively: (a) rf 100 W, (b) dc 100 W, (c) rf 120 W, (d) dc 120 W. (e) Bright-field TEM micrograph from the dc-120 W Mo film.

seen that the AFM results are in good agreement with the SEM images and XRD patterns. For both rf and dc sputtering, the films deposited at a higher power have a rougher surface and a larger grain size. The rf-sputtered films show a lower surface roughness than the respective dc-sputtered films at the same supplied power value. The average RMS roughness of the rf-120 W film is 5.03 nm, much lower than that of the dc-120 W film (16.2 nm), but similar to that of the dc-100 W film (4.96 nm). When considering the reason, besides the grain size, this difference might be partially attributed to the presence of larger voids and porous structure existing in the dc-sputtering films[20]. This conclusion has been further verified by the bright-field TEM micrographs of the dc-120 W film [Fig. 4(e)] where the presence of grain boundary voids is clearly observed and the porous structure is quite dramatic.

In order to investigate the interfacial adhesion between substrate and deposited films, SEM observations of the cross section of the dc and rf films have been taken [Figs. 4(a)–4(d)]. All of the films consist of columnar grains, perpendicular to the substrate, that are suitable for CIGS uses. Compared with the dc-sputtered films, the rf-sputtered films show a closer-packed microstructure. At the supplied power of 100 W, both rf- and dc-sputtered films show a good adhesion between the Mo film and the soda-lime glass substrate. But at the higher sputtering power of 120 W, a narrow gap is present in the interface for the dc sputtering. Contrary to the dc-sputtering case, the rf-sputtered film at rf-120 W still keeps adhesive well to the substrate and there is no noticeable crack.

Adhesive properties between the films and substrates are critical to the performance of thin film solar cells. It is traditionally agreed that the adhesion depends strongly on the Ar pressure in the system[11]. The two-step deposition scheme in our experiments greatly favors the adhesion as follows: the first step at a higher pressure (2.4 Pa) serves as an intermediate layer between the substrate and the Mo films, and the second step at a relatively lower pressure (0.6 Pa) grows the well-crystallized, highly conductive, and surface-textured layer. The high-pressure-based sputtering in the first step produces lower energy Mo atoms and a lower deposition rate, and this initial Mo deposition

can serve as a buffer layer to reduce the stress between the film and the substrate.

What are the underlying reasons for the different film properties between rf and dc sputtering? In the dc magnetron sputtering process, when the higher power is being supplied (say 120 W), the sputtered particles will deposit on the substrate with a high energy and the residue energy promotes the moving and further growth of the particle. This process generates larger Mo grains and good crystallization of the films relative to its counterpart rf sputtering. At the same time, the higher kinetic energy resulting from dc sputtering will definitely impart particles that are less compact and loosen the adhesion between Mo films and the substrate. On the contrary, the electrical source in the case of rf magnetron sputtering is powered at a frequency of 13.56 MHz. This high alternating electrical field not only makes the charged particle ionized and linger longer in the glow discharge regime through bombarding circularly, but engenders multiple gas-phase collisions, reducing the energy of the sputtered atoms and neutralized gas ions. Ultimately, the deposited grains tend to be much finer and more uniform with a smoother film surface and better adhesion to the substrate compared to dc sputtering under the same conditions.

Based on the previous results, the sputtering method and power play great roles in the adhesive property. The dc sputtering process can generate larger grains and better-crystallized films than its counterpart rf sputtering. In the meanwhile, the higher kinetic energy resulting from dc sputtering definitely weakens the adhesion between Mo films and the substrate through "overbombing" the interfacial region. This overbombing will induce over-residue energy to promote the atom migration for further grain growth to form well-crystallized Mo films but possibly without enough buffering adhesion to the substrate. Contrarily, the rf sputtering has a reduced energy of sputtered atoms and neutralized gas ions, which induces less crystallization and smaller grains but gains better adhesion to the substrate even with a high power of 120 W. The above conclusion is clearly supported from the cross-sectional images [Figs. 4(a)–4(d)] of the Mo films deposited from dc and rf sputtering at the same power value. The good adhesion between the Mo film and the soda-lime glass substrate for both the dc-100 W and rf-120 W sputtered films should be attributed to their similar deposition rate and crystallization, as mentioned above.

The sheet resistances and the electrical resistivities of the rf- and dc-sputtered Mo films are listed in Table 1. It can be seen that the resistivity of the Mo film highly depends on the sputtering method and the sputtering power. The electrical resistivity of the Mo film decreases with the increase of the supplied power. The dc-120 W film reaches the lowest resistivity of $1.02 \times 10^{-5}\ \Omega \cdot \mathrm{cm}$ and the lowest sheet resistance of 0.14 Ω. Accordant with the previous structural analysis, the resistivity of the dc films is lower than that of the respective rf films. For example, the dc-100 W has a resistivity and sheet resistance of $2.81 \times 10^{-5}\ \Omega \cdot \mathrm{cm}$ and 0.23 Ω, in contrast to $5.56 \times 10^{-5}\ \Omega \cdot \mathrm{cm}$ and 0.38 Ω for rf-100 W. But both the dc-100 W and rf-120 W films reach a fairly low and similar resistivity and sheet resistance of $2.81 \times 10^{-5}\ \Omega \cdot \mathrm{cm}$ and 0.23 Ω, $2.78 \times 10^{-5}\ \Omega \cdot \mathrm{cm}$ and 0.24 Ω, respectively. The electrical resistance of the Mo film is mainly affected by the properties of grain boundaries. Distorted lattice, unsaturated bonds, and impurity segregation near the grain boundaries become the barriers for charge carriers to transport. These grain boundary barriers suppress carrier motion and decrease the conductivity of the film. The higher-power, no matter in rf sputtering or dc sputtering, will have a larger grain size and better crystallization, and decreases the areas of the grain boundaries. As a result, the Mo films formed in higher power tend to have a lower conductivity. The same mechanism can be applied to explain the resistivity difference between the higher energy dc films and lower energy rf ones.

As the back contact electrode in CIGS solar cells, the Mo film is desired to have a low resistivity value of about 1×10^{-5}–$5 \times 10^{-5}\ \Omega \cdot \mathrm{cm}$. This can be obtainable in the dc-100 W, dc-120 W, and rf-120 W sputtered films. Considering the adhesion requirement to the substrate, the dc-100 W and rf-120 W films are more suitable as the candidates for the contact electrodes of CIGS solar cells.

In order to examine the availability of the optimal Mo films above, the Mo films prepared by dc-100 W and rf-120 W sputtering, respectively, have been used as the back contacts of a CIGS solar cell. The active CIGS layer is with the precursor molar ratio of Cu:In:Ga equaling to 0.95:0.75:0.25. It was prepared by magnetron sputtering on the Mo/glass substrate and further annealed at 500°C in a Se-contained graphite box[21,22]. The representative cross section of the glass/Mo/CIGS is shown in Fig. 5(a). Columnar CIGS grains on the Mo layer were clearly observed, showing the good adhesive interface between the Mo and CIGS layers. Here, the Mo film served not only as the back contact of the hole collector but also as a good adhesive layer between the glass and CIGS.

The characteristic I-V curves of the $0.5\ \mathrm{cm} \times 0.5\ \mathrm{cm}$ CIGS solar cell accomplished with the above two techniques are shown in Fig. 5(b). The photocurrent densities are high, up to 26.1 and $25.97\ \mathrm{mA/cm^2}$ at AM1.5

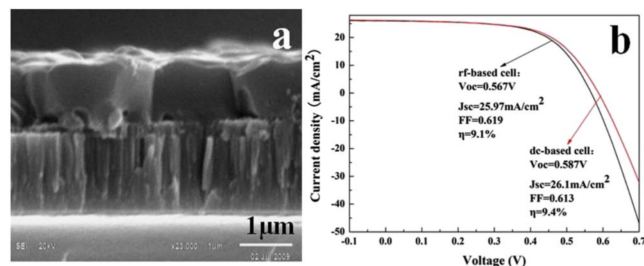

Fig. 5. (a) SEM cross-sectional image of the glass/Mo/CIGS sample after selenization, (b) I-V characteristic of the CIGS solar cells.

illumination (100 mW/cm^2), and efficiencies as high as 9.4% and 9.1% without antireflective films, for dc-based and rf-based cells, respectively. Compared with dc-100 W film, rf-120 W film has the narrower FWHM and larger grain size (as shown in Table 1), which demonstrate the better characterization and much denser microstructure of the rf-120 W film. On the contrary, the looser structure of the dc-100 W film will facilitate the diffusion of Na from the soda-lime glass substrate to the CIGS absorber layer; that is why the higher cell efficiency was obtained. The results confirm that Mo films with the above two techniques are best suitable for application as back contact electrodes of CIGS thin film solar cells.

The Mo thin films are prepared employing a two-step deposition process by magnetron sputtering in order to systematically compare the difference between dc- and rf-based sputtering. The structural, morphological, and electrical properties of the rf- and dc- sputtered Mo films are studied and compared, respectively. For both dc and rf sputtering techniques, surface texture (roughness), columnar grain size, and electrical conductivity of the Mo film increase with increasing sputtering power. But compared with the rf sputtering, dc-based sputtering shows a systematic shift in structural and physical properties of the deposited Mo films. At the same time, both rf and dc techniques can be optimized to satisfy the technical requirements of CIGS solar cells. All of these results will hopefully help greatly to instigate the deep understanding of thin film solar cells among the community.

This work was supported by the National Natural Science Foundation of China under Grant No. 11274328.

References

1. M. A. Green, K. Emery, Y. Hishikawa, W. Warta, and E. D. Dunlop, Prog. Photovolt. Res. Appl. **23**, 805 (2015).
2. W. N. Shafarman and J. E. Phillips, in *Proceedings of Conference Record of the Twenty Fifth IEEE Photovoltaic Specialists Conference* (IEEE, 1996), pp. 917.
3. K. Orgassa, H. W. Schock, and J. H. Werner, Thin Solid Films **431–432**, 387 (2003).
4. Z. H. Li, E. S. Cho, and S. J. Kwon, Appl. Surf. Sci. **257**, 9682 (2011).
5. M. Khan and M. Islam, Semicond. **47**, 1610 (2013).
6. M. Khan, M. Islam, A. Akram, Z. M. Qi, and L. B. Li, Mater. Sci. Semicond. Process. **27**, 343 (2014).
7. H. Cao, C. J. Zhang, and J. H. Chu, Sci. China Technol. Sci. **57**, 947 (2014).
8. S. M. Deambrosis, E. Miorin, F. Montagner, V. Zin, M. Fabrizio, M. Sebastiani, F. Massimi, and E. Bemporad, Surf. Coating. Technol. **266**, 14 (2015).
9. L. Zhang, Q. He, W. L. Jiang, F. F. Liu, C. J. Li, and Y. Sun, Chin. Phys. Lett. **25**, 3452 (2008).
10. P. Chelvanathan, Z. Zakaria, Y. Yusoff, M. Akhtaruzzaman, M. M. Alam, M. A. Alghoul, K. Sopian, and N. Amin, Appl. Surf. Sci. **334**, 129 (2015).
11. A. A. Kadam, N. G. Dhere, P. Holloway, and E. Law, J. Vac. Sci. Technol. A **23**, 1197 (2005).
12. H. Khatri and S. Marsillac, J. Phys. Condens. Matter. **20**, 055206 (2008).
13. D. Rafaja, H. Köstenbauer, U. Mühle, C. Löffler, G. Schreiber, M. Kathrein, and J. Winkler, Thin Solid Films **528**, 42 (2013).
14. X. Y. Dai, A. J. Zhou, L. D. Feng, Y. Wang, J. Xu, and J. Z. Li, Thin Solid Films **567**, 64 (2014).
15. G. Zoppi, N. S. Beattie, J. D. Major, R. W. Miles, and I. Forbes, J. Mater. Sci. **46**, 4913 (2011).
16. A. Marcelli, B. Spataro, S. Sarti, V. A. Dolgashev, S. Tantawi, D. A. Yeremian, Y. Higashi, R. Parodi, A. Notargiacomo, J. Q. Xu, G. Cappuccio, G. Gatti, and G. Cibin, Surf. Coating. Technol. **261**, 391 (2015).
17. J. Tranchant, P. Y. Tessier, J. P. Landesman, M. A. Djouadi, B. Angleraud, P. O. Renault, B. Girault, and P. Goudeau, Surf. Coating. Technol. **202**, 2247 (2008).
18. X. Q. Jiao, J. Yang, R. Zhang, N. Zhang, H. Zhong, and Y. Shi, Mat. Lett. **124**, 318 (2014).
19. D. Y. Wan, F. Q. Huang, X. L. Mou, Y. M. Wang, and F. F. Xu, ACS Appl. Mater. Int. **2**, 2147 (2010).
20. Y. G. Shen, J. Mater. Sci. Eng. **359**, 158 (2003).
21. C. Yang, D. Wan, Z. Wang, and F. Huang, Chin. Opt. Lett. **9**, 103102 (2011).
22. Z. Wang, D. Wan, F. Huang, and F. Xu, Chin. Opt. Lett. **12**, 093101 (2014).